Available online at www.sciencedirect.com
SCIENCE DIRECT
Journal of Solid State Chemistry 179 (2006) 1642–1649
JOURNAL OF SOLID STATE CHEMISTRY
www.elsevier.com/locate/jssc

Crystal growth, transport, and magnetic properties of $Ln_3Co_4Sn_{13}$ (Ln = La, Ce) with a perovskite-like structure

Evan Lyle Thomas[a], Han-Oh Lee[b], Andrew N. Bankston[a], Samuel MaQuilon[b], Peter Klavins[b], Monica Moldovan[c], David P. Young[c], Zachary Fisk[b], Julia Y. Chan[a,*]

[a]Department of Chemistry, Louisiana State University, 232 Choppin Hall, Baton Rouge, LA 70803, USA
[b]Department of Physics, University of California, Davis, CA 95616, USA
[c]Department of Physics and Astronomy, Louisiana State University, Baton Rouge, LA 70803, USA

Received 1 February 2006; accepted 18 February 2006
Available online 29 March 2006

Abstract

$Ln_3Co_4Sn_{13}$ (Ln = La, Ce) have been synthesized by flux growth and characterized by single crystal X-ray diffraction. These compounds adopt the $Yb_3Rh_4Sn_{13}$-type structure and crystallize in the cubic space group $Pm\bar{3}n$ (No. 223) with $Z = 2$. Lattice parameters at 298 K are $a = 9.6430(6)$ Å, $V = 896.68(10)$ Å^3, and $a = 9.6022(5)$ Å, $V = 885.34(8)$ Å^3 for the La and Ce analogues, respectively. The crystal structure consists of an Sn-centered icosahedron at the origin of the unit cell, which shares faces with eight Co trigonal prisms and 12 Ln-centered cuboctahedra. Magnetization data at 0.1 T show paramagnetic behavior down to 1.8 K for $Ce_3Co_4Sn_{13}$, with $\mu_{eff} = 2.56\,\mu_B$ per Ce^{3+}, while conventional type II superconductivity appears below 2.85 K in the La compound. Electrical resistivity and specific heat data for the La compound show a corresponding sharp superconducting transition at $T_c \sim 2.85$ K. The entropy and resistivity data for $Ce_3Co_4Sn_{13}$ show the existence of the Kondo effect with a complicated semiconducting-like behavior in the resistivity data. In addition, a large enhanced specific heat coefficient at low T with a low magnetic transition temperature suggests a heavy-fermionic character for the Ce compound. Herein, the structure and physical properties of $Ln_3Co_4Sn_{13}$ (Ln = La, Ce) are discussed.

Keywords: $Ce_3Co_4Sn_{13}$; $La_3Co_4Sn_{13}$; $Ln_3Co_4Sn_{13}$; $SnLn_3Co_4Sn_{12}$; $SnCe_3Co_4Sn_{12}$; X-ray diffraction; Electrical resistivity; Rare-earth cuboctahedra; Icosahedra; Rare-earth intermetallics; Stannides; Superconductivity; Specific heat; Heavy fermion

1. Introduction

Many ternary stannides, Ln–T–Sn (Ln = Lanthanide; T = Transition metal), exhibit notable physical properties such as Kondo lattice behavior, superconductivity, or long-range magnetic order, and also adopt interesting structures [1]. These compounds display magnetic properties due to either the T or Ln substructure, or both. $La_6Co_{13}Sn$ is a ferromagnet with $T_c = 190$ K, due to the Co substructure, with a Co magnetic moment of $1.1\,\mu_B$ [2]. $LnCo_3Sn$ (Ln = Y, Gd–Yb) possess ordering temperatures of 117–238 K; however, the Co moments are lower than the expected values, a phenomenon which is attributed to the Co clusters found within the structure [3]. In the equiatomic LnRhSn group of compounds, LaRhSn becomes superconducting below 1.7 K [4]. The Kondo system, CeRhSn, shows valence fluctuations [5], and YbRhSn is a heavy fermion with an electronic specific heat coefficient $\gamma \sim 1200\,\mathrm{mJ\,mol^{-1}\,K^{-2}}$ [6–10]. Heavy fermions are materials that possess large enhanced electronic masses ($\gamma \sim 100$ times that of a free electron) as a result of the interactions between the conduction electrons and the local magnetic ions at low temperatures [11,12]. Typically, the Ln atoms in ternary stannides are trivalent (with the exception of some Ce and Yb compounds), and the contribution of the transition metal to the magnetism is minimal. The compositions and structures adopted by these compounds, however, heavily influence their transport properties.

In our search for new Ce-based intermetallics by exploring the La–Co–Sn and Ce–Co–Sn systems, we have synthesized $Ln_3Co_4Sn_{13}$ (Ln = La, Ce) which are isostructural to the

*Corresponding author. Fax: +1 225 578 3458.
E-mail address: jchan@lsu.edu (J.Y. Chan).

0022-4596/$ - see front matter © 2006 Elsevier Inc. All rights reserved.
doi:10.1016/j.jssc.2006.02.024

$Yb_3Rh_4Sn_{13}$-type stannides first reported by Hodeau et al. [13]. The coexistence of magnetism and superconductivity ($T_c \sim 8$ K) has been observed in $Yb_3Rh_4Sn_{13}$ [13,14], while heavy fermion behavior with two phase transitions is observed in $Ce_3Ir_4Sn_{13}$ [15–17]. Furthermore, the isostructural $Ce_3Pt_4In_{13}$, is also a heavy fermion with $\gamma \sim 1000\,mJ\,mol^{-1}\,K^{-2}$ [18]. The crystal structure of the $Ln_3Co_4Sn_{13}$ (Ln = La–Nd, Sm, Gd, Tb) compounds has been previously studied by powder X-ray diffraction methods [19]. Herein we report the synthesis, structure characterization by single crystal X-ray diffraction, magnetization, electrical resistivity and specific heat of $Ln_3Co_4Sn_{13}$ (Ln = La, Ce) and compare the structures and physical properties to the Rh and Ir analogues [15,20].

2. Experimental

2.1. Synthesis

$Ln_3Co_4Sn_{13}$ (Ln = La, Ce) single crystals were grown using excess Sn. Ingots of La or Ce (99.99% purity, Materials Preparation Center, Ames Laboratory), Co powder (99.998% purity, Alfa Aesar), and Sn shot (99.8% purity, Alfa Aesar) were weighed and placed into alumina crucibles in a 1:1:20 (Ln:Co:Sn) ratio. The samples, weighing nearly 3.25 g, were covered with quartz wool and encapsulated into evacuated, fused-silica tubes. They were heated to 1273 K for 5 h, then cooled to 1123 K at a rate of 75 K h^{-1}, and finally cooled to 523 K at a rate of 33 K h^{-1}. At this temperature, the ampoules were removed from the furnace and the excess Sn was removed by centrifugation. The retrieved irregularly shaped crystals, with dimensions between 1 and 2 mm^3, were slightly air and moisture sensitive, as surface oxidation appeared following exposure to the atmosphere for extended periods. The centrifugation process removed most of the flux contamination on the surfaces of the single crystals; however, where necessary, the remaining topical flux was etched using concentrated HCl. Powder X-ray diffraction data were collected using a Bruker D-8 X-ray diffractometer with monochromatized CuK_α radiation, $\lambda = 1.540562$ Å. Phase identification of the $Ln_3Co_4Sn_{13}$ (Ln = La, Ce) compounds was determined by comparing the powder patterns (not shown) taken from ground single crystals with that of $Yb_3Rh_4Sn_{13}$ [13] and also with the calculated powder pattern from the refined crystal structure of $Ce_3Co_4Sn_{13}$. Multiple crystals from the products of both reactions were also characterized by single crystal X-ray diffraction as a check for homogeneity.

2.2. Single crystal X-ray diffraction

Suitable crystal fragments with dimensions of $\sim 0.025 \times 0.050 \times 0.050\,mm^3$ ($La_3Co_4Sn_{13}$) and $\sim 0.025 \times 0.10 \times 0.10\,mm^3$ ($Ce_3Co_4Sn_{13}$) were mechanically separated and glued to the tip of a glass fiber with epoxy. Structural analysis was done using a Nonius Kappa CCD diffractometer equipped with graphite monochromated MoK_α radiation ($\lambda = 0.70173$ Å) at room temperature and at 140 K (to check for a structural phase transition in the Ce compound). Additional data collection parameters are presented in Table 1. The structures were solved by direct methods and refined using the SHELXL97 package [21]. The atomic data reported for $Yb_3Rh_4Sn_{13}$ [13] were used to further refine the structural models. Data were corrected for extinction and refined with anisotropic atomic displacement parameters. To accurately determine the composition of our compounds, the occupancy parameters were refined in separate sets of least-squares cycles, since $Yb_3Rh_4Sn_{13}$-type stannides may show defects at the origin of the unit cell (Sn1 on the 2a site) as observed in $Ce_3Rh_4Sn_{13}$ and $Ce_3Ir_4Sn_{13}$ [20]. Unlike the Rh and Ir analogues, the Sn1 sites in $Ln_3Co_4Sn_{13}$ (Ln = La, Ce) are fully occupied. The atomic positions and structural information for both compounds are detailed in Table 2. Table 3 lists selected interatomic distances. Lattice parameters obtained from the room-temperature data collections are $a = 9.6430(6)$ and 9.6022(5) Å, for the La and Ce compounds, respectively. These values are in close agreement with data reported previously from powder X-ray diffraction: 9.635(1) Å (La) and 9.594(1) Å (Ce) [19]; and 9.721 Å (La) and 9.590 Å (Ce) [22]. The final least-squares refinement cycle gave $R(F) = 0.0305$ (La) and 0.0561 (Ce) and $R_w(F_o^2) = 0.0560$ (La) and 0.1424 (Ce). The largest differences in the Fourier map from the room-temperature data collections are 1.658/−1.905 e Å^{-3} from La/Sn2 in the La compound and 3.615/−2.506 e Å^{-3} from Ce/Sn1 in the Ce compound. Additional crystallographic information in CIF format is provided as Supporting Information.

2.3. Physical property measurements

Magnetic data were measured on single crystals using a Quantum Design MPMS Superconducting Quantum Interference Device magnetometer. The zero-field-cooled (ZFC) temperature-dependent susceptibility data were taken in an applied field of 0.1 T up to room temperature after being cooled to 1.8 K under zero magnetic field. The field-dependent susceptibility was measured at 2 K by sweeping the magnetic field to 7 T and back. The resistivity data have been measured using a standard four-probe method down to 0.4 K with a Quantum Design Physical Property Measurement System (PPMS) at ambient pressure. The specific heat was measured with a Quantum Design PPMS using a thermal relaxation method from 0.36 to 30 K in zero applied field; entropy was calculated by integrating the specific heat divided by the temperature.

3. Results and discussion

3.1. Structure

$Ln_3Co_4Sn_{13}$ (Ln = La, Ce) crystallize in the $Pm\bar{3}n$ space group (No. 223) with the $Yb_3Rh_4Sn_{13}$ structure-type [13].

Table 1
Structural refinement data for $Ln_3Co_4Sn_{13}$ (Ln = La, Ce)

Formula	$La_3Co_4Sn_{13}$	$Ce_3Co_4Sn_{13}$	$Ce_3Co_4Sn_{13}$
Formula weight	2195.42	2199.05	2199.05
Space group	$Pm\bar{3}n$	$Pm\bar{3}n$	$Pm\bar{3}n$
a (Å)	9.6430(6)	9.6022(5)	9.5810(6)
V (Å^3)	896.68(10)	885.34(8)	879.49(10)
Z	2	2	2
Crystal dimensions (mm^3)	$0.025 \times 0.050 \times 0.050$	$0.025 \times 0.10 \times 0.10$	$0.025 \times 0.10 \times 0.10$
Temperature (K)	298(2)	298(2)	140(2)
Calculated density (g cm^{-3})	8.131	8.250	8.304
θ range (deg)	2.99–29.99	3.00–29.95	3.01–30.03
Absorption coefficient (mm^{-1})	28.253	29.091	29.283
Collected reflections	767	770	761
Unique reflections	259	258	258
R_{int}	0.0491	0.0474	0.0436
h	$-13 \leqslant h \leqslant 13$	$-13 \leqslant h \leqslant 13$	$-13 \leqslant h \leqslant 13$
k	$-9 \leqslant k \leqslant 9$	$-9 \leqslant k \leqslant 9$	$-9 \leqslant k \leqslant 9$
l	$-8 \leqslant l \leqslant 9$	$-9 \leqslant l \leqslant 9$	$-9 \leqslant k \leqslant 9$
Data/parameters/restraints	259/13/0	258/13/0	258/13/0
Goodness of fit on F_o^2	1.135	1.131	1.149
$R(F)$ for $F_o^2 > 2\sigma(F_o^2)$ [a]	0.0305	0.0561	0.0432
$R_w(F_o^2)$ [b]	0.0560	0.1424	0.1060
Extinction coefficient	0.0053(7)	0.0038(9)	0.0043(6)
$\Delta\rho_{max}$ (e Å^{-3})/$\Delta\rho_{min}$ (e Å^{-3})	1.658/−1.905	3.615/−2.506	2.765/−2.201

[a] $R(F) = \sum ||F_o| - |F_c|| / \sum |F_o|$.
[b] $R_w(F_o^2)\left[\sum [w(F_o^2 - F_c^2)^2] \Big/ \sum [w(F_o^2)^2]\right]^{1/2}$.

Table 2
Atomic positions, site symmetry and U_{eq} values for $Ln_3Co_4Sn_{13}$ (Ln = La, Ce)

Atom	Wyckoff site	x	y	z	U_{eq} (Å^2)[a]
$La_3Co_4Sn_{13}$					
Sn1	2a	0	0	0	0.0184(5)
La	6d	1/4	1/2	0	0.0133(3)
Co	8e	1/4	1/4	1/4	0.0113(5)
Sn2	24k	0	0.30189(8)	0.15684(7)	0.0178(3)
$Ce_3Co_4Sn_{13}$ (298 K)					
Sn1	2a	0	0	0	0.0151(8)
Ce	6d	1/4	1/2	0	0.0101(6)
Co	8e	1/4	1/4	1/4	0.0085(7)
Sn2	24k	0	0.30286(10)	0.15688(9)	0.0142(5)
$Ce_3Co_4Sn_{13}$ (140 K)					
Sn1	2a	0	0	0	0.0098(7)
Ce	6d	1/4	1/2	0	0.0075(5)
Co	8e	1/4	1/4	1/4	0.0063(7)
Sn2	24k	0	0.30306(10)	0.15681(9)	0.0113(4)

[a] U_{eq} is defined as one-third of the trace of the orthogonalized U_{ij} tensor.

The Sn1, Ln, Co, and Sn2 atoms occupy the 2a, 6d, 8e, and 24k sites, respectively. The structure of $Ce_3Co_4Sn_{13}$ is shown in Fig. 1 and is similar to the $A'A''_3B_4O_{12}$-type ($Im\bar{3}$, No. 204) compounds such as $[CaCu_3](Ge_4)O_{12}$ [23] and $ACu_3Ti_4O_{12}$ [24]. $Ln_3Co_4Sn_{13}$ (Ln = La, Ce) have a perovskite-like arrangement where the Sn and Ln atoms occupy the A site of the perovskite and Co occupies the B site [13,25,26]. The $Ln_3Co_4Sn_{13}$ (Ln = La, Ce) compounds extend the $Yb_3Rh_4Sn_{13}$-type family of compounds with three substructures such that the Sn1 atoms form $Sn1(Sn2)_{12}$ icosahedra, the Ln atoms form $Ln(Sn2)_{12}$ cuboctahedra, and the transition metal forms TSn_6 trigonal prisms. Additionally, it can also be regarded as the sum of two interpenetrating structures of $SnLn_3$ and $CoSn_3$.

The Sn1 atoms occupy the origin of the unit cell and form an infinite network of edge-sharing $Sn1(Sn2)_{12}$ icosahedra which pack in an CsCl arrangement. The faces of each Sn1 icosahedron in the network make contact with

Table 3
Selected interatomic distances (Å) in $Ln_3Co_4Sn_{13}$ (Ln = La, Ce)

	La	Ce (298 K)	Ce (140 K)
Sn icosahedron			
Sn1–Sn2 (× 12)	3.2806(7)	3.2751(10)	3.2693(10)
Ln cuboctahedron			
Ln–Sn2 (× 4)	3.3470(6)	3.3335(9)	3.3272(9)
Ln–Sn2 (× 8)	3.4274(4)	3.4080(7)	3.3992(6)
Co trigonal prism			
Co–Sn2 (× 6)	2.6210(3)	2.6114(4)	2.6063(4)

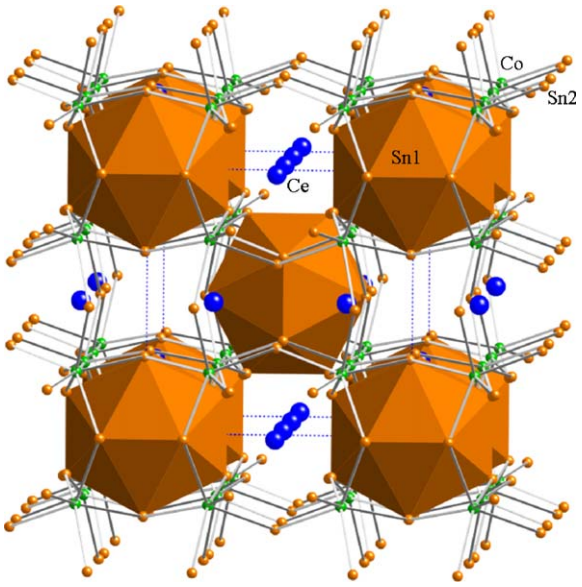

Fig. 1. The structure of $Ce_3Co_4Sn_{13}$ highlighting the arrangement of the $Sn1(Sn2)_{12}$ icosahedra (light gray), with Co atoms (black circles) bonding to Sn2 atoms (white circles) forming trigonal prisms. For simplicity, Ce (dark gray circles) is represented as isolated atoms.

eight $CoSn_6$ trigonal prisms and 12 *Ln*-centered cuboctahedra. The Sn1–Sn2 distances are 3.2806(7) Å (× 12) for $La_3Co_4Sn_{13}$ and 3.2751(10) Å (× 12) for $Ce_3Co_4Sn_{13}$. For comparison, the Sn1–Sn2 distances found in the Rh and Ir analogues are 3.342 and 3.349 Å, respectively [20]. These distances are slightly larger than the Sn–Sn distances found in β-Sn (4 × 3.02 and 2 × 3.18 Å) [27].

Within the structure of $Ce_3Co_4Sn_{13}$, there is a clustered network of lanthanide cuboctahedra [$Ln(Sn2)_{12}$] which are both face- and edge-sharing. There are two different *Ln*–Sn2 distances: 8 × *Ln*–Sn2 distances of 3.4274(4) and 3.4080(7) Å for Ln = La and Ce, respectively, and 4 × *Ln*–Sn2 interatomic distances of 3.3467(7) and 3.3335(9) Å for Ln = La and Ce, respectively. By comparing the Ce–Sn2 cuboctahedral distances of the $Ce_3T_4Sn_{13}$ (T = Co, Rh, Ir) compounds, we observe that the Rh analogue is the least distorted [20], with the ratio of *Ln*–Sn1 to *Ln*–Sn2 contacts closest to unity. It is worthwhile to note that similar trends are also found in the $LnTIn_5$ (Ln = La, Ce; T = Co, Rh, Ir) [28] and Ln_2TIn_8 (Ln = La, Ce; T = Rh, Ir) compounds [29]. Both structures contain *Ln* cuboctahedra with 8-fold *Ln*–In and 4-fold *Ln*–In distances and the cuboctahedra in the Rh analogues are the least distorted.

The $Co(Sn2)_6$ trigonal prisms found in $Ln_3Co_4Sn_{13}$ (Ln = La, Ce) are shown in Fig. 2. They are corner-sharing with a tilted three-dimensional arrangement that creates "cages" which encompass the Sn1 atoms. This feature is similar to the BO_6 octahedra in $A'A''_3B_4O_{12}$-type compounds and also to the TPn_6 (Pn = pnictogen) octahedra found in the structures of skutterudites such as $LaFe_4P_{12}$ [30]. The trigonal prisms contain Co–Sn interatomic distances of 2.6210(3) Å (× 6) and 2.751(10) Å (× 6) for Ln = La and Ce, respectively. These distances are slightly less than the sum of the covalent radii of Co (1.25 Å) and Sn (1.54 Å); however, similar distances are found in the Co–Sn binaries CoSn (2.618 and 2.639 Å) [31], $CoSn_2$ (2.737 Å) [32], and Co_3Sn_2 (2.703 Å) [33]. The *T*–Sn interatomic distance in the isostructural $Ce_3Rh_4Sn_{13}$ and $Ce_3Ir_4Sn_{13}$ compounds are 2.659 and 2.667 Å, respectively, which are also slightly shorter than the sum of the metallic radii, although larger than the sum of the ionic radii [20]. In addition, the Rh–Sn2 distances in $Yb_3Rh_4Sn_{13}$ are also shorter than the corresponding intermetallic radii and it has been suggested that the bonding nature in this compound may be "covalent-ionic" [13]. Given the similar crystal chemistry found in the $A'A''B_4O_{12}$ compounds, our $Ce_3Co_4Sn_{13}$ compound may be interpreted as the covalent counterpart to $A'A''B_4O_{12}$.

3.2. Physical properties

The magnetic susceptibility (χ) of a single crystal of $Ce_3Co_4Sn_{13}$ shows Curie–Weiss paramagnetic behavior down to 1.8 K with an applied field of 0.1 T. This is consistent with the data reported by Israel et al. [22].

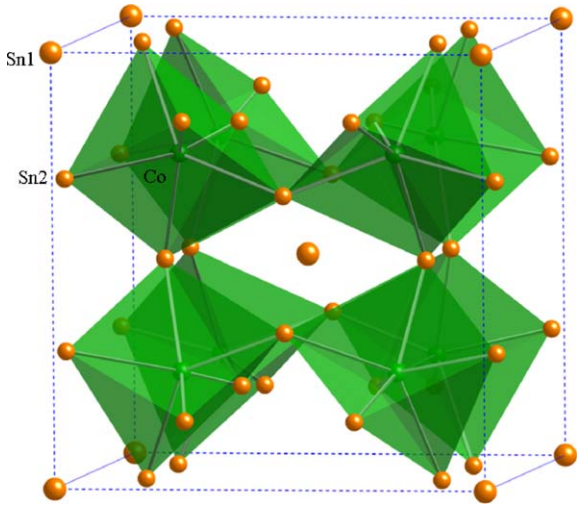

Fig. 2. Projection of the Co substructure with corner-sharing $Co(Sn2)_6$ trigonal prisms. The Co atoms are black with Sn atoms represented as gray. Bonds between the Sn1 and Sn2 atoms have been omitted for clarity.

A Curie–Weiss fit, defined by the equation $1/\chi = (1/C)T - \theta_{cw}/C$, applied to the inverse susceptibility data in the temperature region above 100 K gives a negative Weiss temperature (θ_{cw}) of −37 K, indicating an antiferromagnetic correlation due to the Kondo effect. The effective moment (μ_{eff}) from the Curie constant C is 2.56 μ_B/Ce, which is close to the theoretical value of 2.54 μ_B for the Ce^{3+} free ion and similar to the previously reported moment of 2.58(2) μ_B [22]. This, along with the fact that La analogue behaves as a Pauli paramagnet, suggests that the magnetic contribution comes from Ce, and Co does not carry a magnetic moment in $Ce_3Co_4Sn_{13}$. For comparison, the effective moments reported for the Rh and Ir analogues are $\mu_{eff} = 2.45(2)\,\mu_B$ [20] and 2.45 μ_B [15], respectively. The field-dependent magnetization data, $M(H)$, at 2 K for $Ce_3Co_4Sn_{13}$ are shown in Fig. 3a. The data fit well with a doubly degenerate ground state yielding $\mu_{sat} = gJ_z\,\mu_B$ of 0.64 μ_B/Ce.

Fig. 3b shows the magnetic data for $La_3Co_4Sn_{13}$. A superconducting signal is detected below 2.85 K with constant Pauli paramagnetic behavior above this temperature. The type II superconductor behavior with H_{c1}∼20 G and an upper critical field (H_{c2})∼1 T (not shown), is most likely conventional BCS superconductivity mediated by the vibration of the lattice. Perfect diamagnetism is expected in the superconducting state below H_{c1}, which is represented by the susceptibility value ($4\pi M/H$) of −1 or $4\pi M$ is equal to $-H$. The data clearly show a full Meissner effect, and no superconductivity from Sn inclusions has been detected in this particular sample.

Electrical resistivity data for $La_3Co_4Sn_{13}$ are shown in Fig. 4a. The resistivity suddenly drops to zero in the La compound at T_c∼2.8 K due to the superconducting transition, consistent with the susceptibility data. (Israel et al. report a $T_c = 2.4$ K; however, no transport data were presented due to Sn flux contamination [22].) Above T_c, the resistivity increases as T^3, consistent with Wilson's theory of the s–d hybridization effect in transition metals [34]. In addition, there is a shoulder between 10 and 160 K. This can be attributed to the s–d scattering between the conduction electrons and electrons from the unfilled Co d-band [35,36]. At higher temperatures, the resistivity rises less rapidly than the usual linear dependence in temperature, which can be related to the high-temperature saturation of the resistance where the electron mean free path is similar to the interatomic distance [37]. The temperature dependence of the resistivity of $Ce_3Co_4Sn_{13}$, shown in Fig. 4b, is very peculiar. With decreasing temperature, $Ce_3Co_4Sn_{13}$ displays metallic behavior down to ∼160 K. A sudden kink at 160 K is observed, which could be due to a structural change. A single crystal X-ray diffraction experiment at 140 K, however, shows no change in the crystal structure from that of the 298 K data as shown in Tables 1–3. Thus, it must be an intrinsic behavior which we do not fully understand at present. Below 160 K, the resistivity shows a rather complicated semiconducting behavior. There are two slope changes between 20 and 150 K which may have the same origin as in the La compound. Below 20 K, the resistivity increases dramatically and a kink is observed at T∼0.6 K corresponding to the transition observed in the specific heat data (∼0.65 K) [38]. We subtracted the resistivity of the La compound from the resistivity of the Ce compound to isolate the magnetic contribution of the Ce f-moment, assuming that lattice and electronic contributions are the same as in the La compound, other than f-electron contribution. As seen in Fig. 5a, above 160 K, one can clearly see the linear behavior in log T, which is indicative of Kondo scattering at high temperature. Below the slight kink at 160 K, only a limited region follows the log T dependence. This feature below 100 K may be due to Kondo scattering along with magnetic fluctuations. We note that there was some

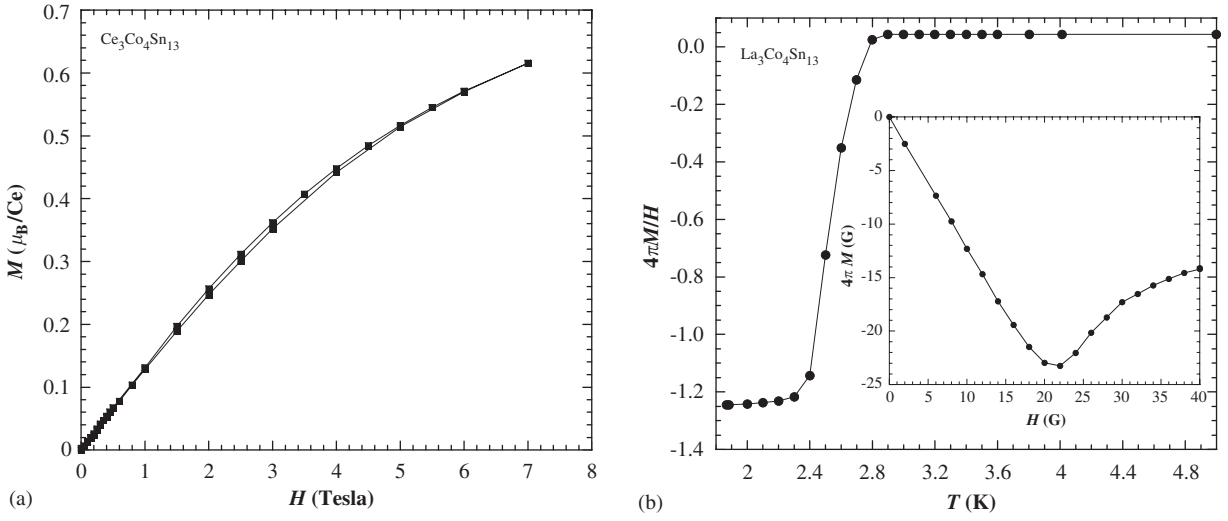

Fig. 3. (a) Field-dependent magnetization, $M(H)$, for $Ce_3Co_4Sn_{13}$ at $T = 2$ K. (b) Zero-field-cooled (ZFC) magnetic susceptibility (χ) as a function of temperature (T) in a magnetic field of $H = 10$ G for an $La_3Co_4Sn_{13}$ single crystal. (Inset) Field-dependent magnetization, $M(H)$, for $La_3Co_4Sn_{13}$ at $T = 2$ K.

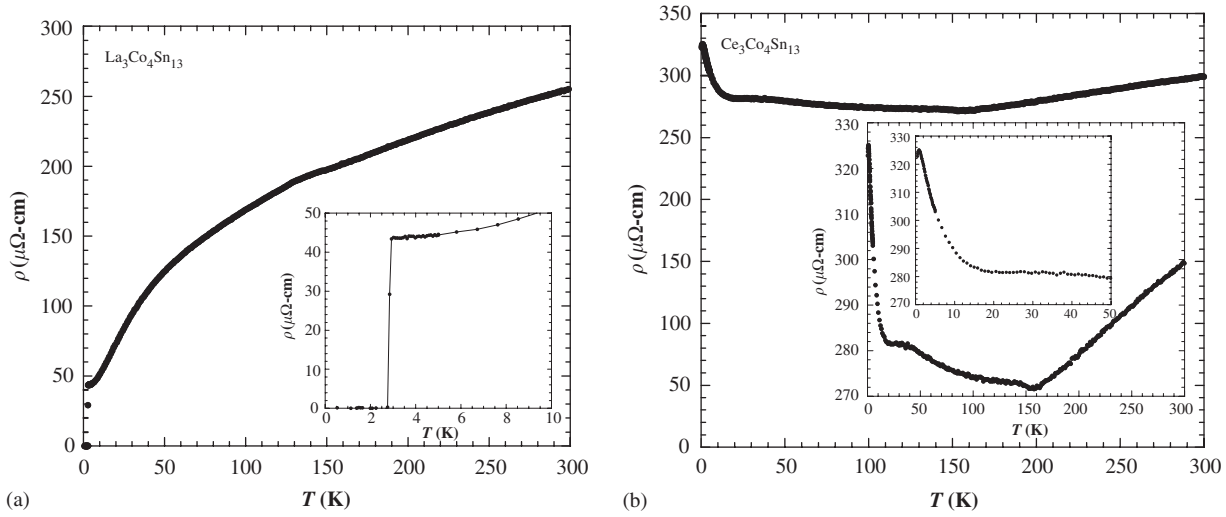

Fig. 4. (a) Temperature-dependence of the electrical resistivity, $\rho(T)$, for $La_3Co_4Sn_{13}$. The inset shows the low-temperature portion of the $\rho(T)$ with a solid line drawn to depict the sharp transition to the superconducting state at $T_c \sim 2.8$ K. (b) The $\rho(T)$ for $Ce_3Co_4Sn_{13}$ with insets showing the transitions at low temperatures.

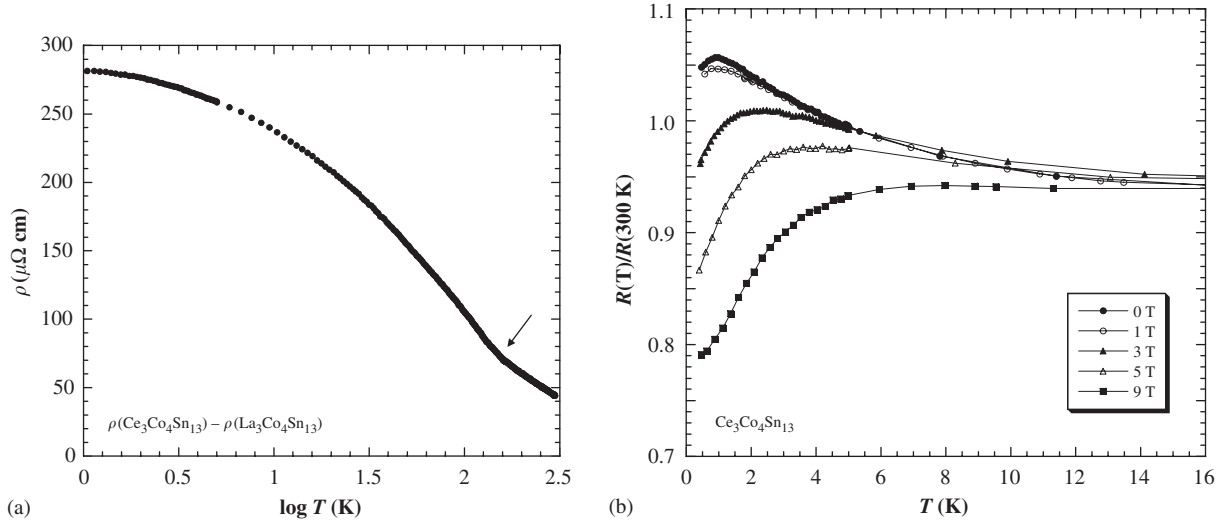

Fig. 5. (a) Resistivity data for $Ce_3Co_4Sn_{13}$ with subtracted $La_3Co_4Sn_{13}$ contribution is plotted on a logarithmic temperature scale. The arrow shows the change in slope. (b) Relative resistance with respect to the temperature at applied magnetic fields of 0 T (closed circles), 1 T (open circles), 3 T (closed triangles), 5 T (open triangles) and 9 T (closed squares).

difficulty in collecting reliable resistivity data due to the Sn inclusions inside the crystal which led to significant changes in resistivity behavior proportional to the amount of the Sn inclusion. The resistivity data presented here for $Ce_3Co_4Sn_{13}$ were reproducible from measurements on several single crystals that had no Sn inclusions.

The negative θ_{cw} from the susceptibility of $Ce_3Co_4Sn_{13}$ suggests an antiferromagnetic nature for this transition. The character of the magnetic transition, however, is not obvious as no long-range order has been detected at 0.8 K from powder neutron diffraction experiments [38]. Moreover, in the specific heat data under applied magnetic field of 2.5 T or more, this kink, originating presumably from short-range magnetic order, is suppressed, and Kondo impurity behavior appears [38]. Resistivity measurements with an applied magnetic field perpendicular to the current were performed to give better insight to the origin of this magnetic transition at low temperature and is shown in Fig. 5b. Interestingly, the kink at low temperatures disappears, and the resistance at 0.4 K drops linearly with applied magnetic field and decreases ~20% with applied field of 9 T. It would be interesting to investigate with higher magnetic fields in order to suppress the low-temperature resistivity to determine if the coherent scattering can be recovered.

Temperature-dependent specific heat divided by the temperature (C_p/T) for $Ce_3Co_4Sn_{13}$ and $La_3Co_4Sn_{13}$ have been measured, and are roughly consistent with behavior

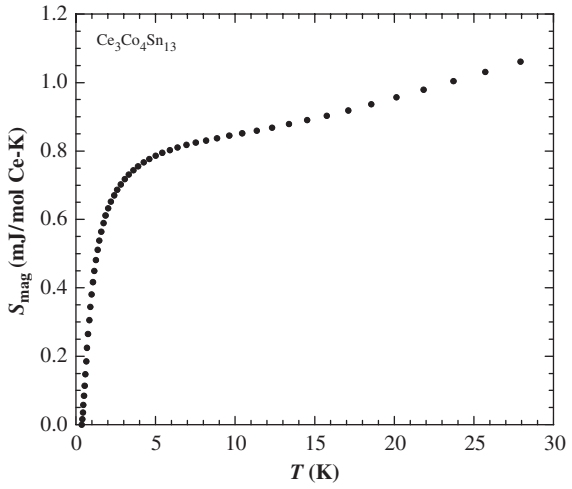

Fig. 6. Entropy of $Ce_3Co_4Sn_{13}$ obtained by integrating C/T of $Ce_3Co_4Sn_{13}$ after subtracting the corresponding $La_3Co_4Sn_{13}$ data.

from previous reported data [22,38]. The linear specific heat coefficient (γ) can be estimated by fitting the data with $\gamma + \beta T^2$ above the transition temperature, giving $\sim$4 mJ mol^{-1} K^{-2} for $La_3Co_4Sn_{13}$. Below 5 K in $Ce_3Co_4Sn_{13}$, C_p/T increases dramatically due to magnetic short-range fluctuations followed by a peak at $\sim$0.65 K, indicating a magnetic phase transition. Although γ estimated from extrapolating C_p/T to zero temperature is about 75 mJ mol^{-1} K^{-2} in the Ce compound, C_p/T is enhanced up to 4280 mJ mol^{-1} K^{-2} at the transition peak temperature. This large enhancement of C_p/T can be caused by large short-range magnetic fluctuations, but evidences of Kondo scattering in the susceptibility, resistivity, and entropy data (to be discussed in a later communication) support a heavy mass state involved in this low-temperature behavior. One can isolate the magnetic part of the specific heat of $Ce_3Co_4Sn_{13}$ by subtracting the corresponding $La_3Co_4Sn_{13}$ data in the normal state to exclude lattice contributions. The corresponding entropy is obtained by integrating C_p/T after subtraction and is shown in Fig. 6. The magnetic entropy should have an $R\ln 2$ value at the transition temperature if the spin is doubly degenerate, i.e., two spin degrees of freedom in its ground state. The magnetic entropy recovered at 10 K is about $0.85R\ln 2$. This value, close to $R\ln 2$, implies the ground state is doubly degenerate as discussed earlier in relation to the magnetization results. The reduction of the entropy from $R\ln 2$ around the transition temperature suggests the existence of the Kondo effect, as indicated from the resistivity data. This value is larger than the previously reported magnetic entropy at 20 K which is 60–70% of $R\ln 2$ [22].

4. Summary

We have synthesized the $Ln_3Co_4Sn_{13}$ (Ln = La, Ce) compounds in single crystalline form, characterized their structures by single crystal X-ray diffraction, and investigated their magnetic and transport properties. Specific heat data show evidence for heavy mass behavior in $Ce_3Co_4Sn_{13}$ and a magnetic phase transition at $T\sim$0.65 K. $La_3Co_4Sn_{13}$ becomes superconducting at $T_c\sim$2.8 K, while transport behavior for the Ce analogue is more complex and contains both a metallic and semiconducting character. $Ln_3Co_4Sn_{13}$ (Ln = La, Ce) is a phase worth further investigation because of the similarity of the structural units (cuboctahedra) found in this phase and the $CeTIn_5$ and Ce_2TIn_8 (M = Co, Rh, Ir) compounds. The heavy fermionic nature along with the low magnetic transition temperature makes $Ce_3Co_4Sn_{13}$ a particularly interesting candidate for the study of magnetic quantum critical phenomena. The behavior of the magnetic field dependence is worth further investigation. Also, thermal transport measurements, such as thermal conductivity and thermoelectric power, may prove interesting due to the caged structure of these materials.

Acknowledgments

J.Y.C. acknowledges the PRF-G, NSF Career (DMR 0237664) and Alfred P. Sloan Fellowship for partial support of this project. Z.F., S.M., and H.L. acknowledge DMR-NSF 0433560 for partial support of this project.

Supporting Information Available: Additional information in CIF format. This material is available free of charge via the Internet at http://pubs.acs.org.

References

[1] R.V. Skolozdra, in: K.A. Gschneidner, L. Eyring (Eds.), Handbook on the Physics and Chemistry of Rare Earths, vol. 24, Elsevier, Netherlands, 1997, p. 399.
[2] F. Weitzer, A. Leithe-Jasper, P. Rogl, K. Hiebl, H. Noël, G. Wiesinger, W. Steiner, J. Solid State Chem. 104 (1993) 368.
[3] R.V. Skolozdra, Stannides of Rare Earth and Transition Metals, Svit, Lviv, Ukraine, 1993.
[4] F. Canepa, S. Cirafici, J. Alloys Compd. 232 (1996) 71.
[5] C.D. Routsi, J.K. Yakinthos, H. Gamari-Seale, J. Magn. Magn. Mater. 117 (1992) 79.
[6] D. Kaczorowski, A. Leithe-Jasper, P. Rogl, H. Flandorfer, T. Cichorek, R. Petri, B. Andraka, Phys. Rev. B 60 (1999) 422.
[7] K. Katoh, G. Terui, Y. Niide, H. Aoki, A. Ochiai, Physica B 261 (1999) 161.
[8] O. Trovarelli, C. Geibel, R. Cardoso, S. Mederle, R. Borth, B. Buschinger, F.M. Grosche, Y. Grin, G. Sparn, F. Steglich, Phys. Rev. B 61 (2000) 9467.
[9] R. Pietri, B. Andraka, D. Kaczorowski, A. Leithe-Jasper, P. Rogl, Phys. Rev. B 61 (2000) 12169.
[10] B. Andraka, R. Pietri, D. Kaczorowski, A. Leithe-Jasper, P. Rogl, J. Appl. Phys. 87 (2000) 5149.
[11] Z. Fisk, H.R. Ott, T.M. Rice, J.L. Smith, Nature 320 (1986) 124.
[12] Z. Fisk, D.W. Hess, C.J. Pethick, D. Pines, J.L. Smith, J.D. Thompson, J.O. Willis, Science 239 (1988) 33.
[13] J.L. Hodeau, J. Chenavas, M. Marezio, J.P. Remeika, Solid State Commun. 36 (1980) 839.
[14] J.P. Remeika, G.P. Espinosa, A.S. Cooper, H. Barz, J.M. Rowell, D.B. McWhan, J.M. Vandenberg, D.E. Moncton, Z. Fisk, L.D. Woolf, H.C. Hamaker, M.B. Maple, G. Shirane, W. Thomlinson, Solid State Commun. 34 (1980) 923.

[15] H. Sato, T. Fukuhara, S. Iwakawa, Y. Aoki, I. Sakamoto, S. Takayanagi, N. Wada, Physica B 188 (1993) 630.
[16] S. Takayanagi, H. Sato, T. Fukuhara, N. Wada, Physica B 199 (1994) 49.
[17] C. Nagoshi, H. Sugawara, Y. Aoki, S. Sakai, M. Kohgi, H. Sato, T. Onimaru, T. Sakakibara, Physica B 359 (2005) 248.
[18] M.F. Hundley, J.L. Sarrao, J.D. Thompson, R. Movshovich, M. Jaime, C. Petrovic, Z. Fisk, Phys. Rev. B 65 (2002) 024401.
[19] R.V. Skolozdra, I.V. Yasnitskaya, O.E. Koretskaya, L.G. Aksel'rud, Dopov. Akad. Nauk Ukr. RSR, Ser. B 6 (1983) 42.
[20] D. Niepmann, R. Pöttgen, K.M. Poduska, F.J. DiSalvo, H. Trill, B.D. Mosel, Z. Naturforsch. B 56 (2001) 1.
[21] G.M. Sheldrick, SHELXL-97, Program for Refinement of Crystal Structures, Göttingen, Germany, 1997.
[22] C. Israel, E.M. Bittar, O.E. Agüero, R.R. Urbano, C. Rettori, I. Torriani, P.G. Pagliuso, N.O. Moreno, J.D. Thompson, M.F. Hundley, J.L. Sarrao, H.A. Borges, Physica B 359 (2005) 251.
[23] Y. Ozaki, M. Ghedira, J. Chenavas, J.C. Joubert, M. Marezio, Acta Crystallogr. B—Struct. Commun. 33 (1977) 3615.
[24] B. Bochu, M.N. Deschizeaux, J.C. Joubert, A. Collomb, J. Chenavas, M. Marezio, J. Solid State Chem. 29 (1979) 291.
[25] S. Miraglia, J.L. Hodeau, M. Marezio, C. Laviron, M. Ghedira, G.P. Espinosa, J. Solid State Chem. 63 (1986) 358.
[26] M. O'Keefe, B.G. Hyde, Acta Crystallogr. B—Struct. Commun. 33 (1977) 3802.
[27] J. Donohue, The Structures of the Elements, Wiley, New York, 1974.
[28] R.T. Macaluso, J.L. Sarrao, P.G. Pagliuso, N.O. Moreno, R.G. Goodrich, D.A. Browne, F.R. Fronczek, J.Y. Chan, J. Solid State Chem. 166 (2002) 245.
[29] R.T. Macaluso, J.L. Sarrao, N.O. Moreno, P.G. Pagliuso, J.D. Thompson, F.R. Fronczek, M.F. Hundley, A. Malinowski, J.Y. Chan, Chem. Mater. 15 (2003) 1394.
[30] W. Jeitschko, D. Braun, Acta Crystallogr. B—Struct. Commun. 33 (1977) 3401.
[31] O. Nial, Z. Anorg. Allg. Chem. 238 (1938) 287.
[32] E.E. Havinga, P. Hokkelin, H. Damsma, J. Less-Common Met. 27 (1972) 169.
[33] H. Rajeswar, H. Manohar, Indian J. Pure Appl. Phys. 8 (1970) 363.
[34] A.H. Wilson, Proc. R. Soc. London, Ser. A 167 (1938) 580.
[35] Z. Fisk, G.W. Webb, Phys. Rev. Lett. 36 (1976) 1084.
[36] M. Weger, R.A. Degroot, F.M. Mueller, M. Kaveh, J. Phys. F 14 (1984) L207.
[37] M. Gurvitch, Phys. Rev. B 24 (1981) 7404.
[38] A.L. Cornelius, A.D. Christianson, J.L. Lawrence, V. Fritsch, E.D. Bauer, J.L. Sarrao, J.D. Thompson, P.G. Pagliuso, Physica B, 2005, submitted for publication.